Journal of Alloys and Compounds 489 (2010) 415–420

Contents lists available at ScienceDirect

Journal of Alloys and Compounds

journal homepage: www.elsevier.com/locate/jallcom

The role of trace element segregation in the eutectic modification of hypoeutectic Al–Si alloys

K. Nogita [a,b,*], H. Yasuda [b], M. Yoshiya [b], S.D. McDonald [a,c], K. Uesugi [d], A. Takeuchi [d], Y. Suzuki [d]

[a] Department of Materials Engineering, The University of Queensland, Brisbane, QLD 4072, Australia
[b] Department of Adaptive Machine Systems, Osaka University, Suita, Osaka, 565-0871, Japan
[c] CRC for Alloy and Solidification Technology (CAST), Brisbane, QLD 4072, Australia
[d] Japan Synchrotron Radiation Research Institute, SPring-8, Sayo, Hyogo, 679-5198, Japan

ARTICLE INFO

Article history:
Received 28 August 2009
Received in revised form
19 September 2009
Accepted 23 September 2009
Available online 2 October 2009

Keywords:
Metals and alloys
Crystal growth
Microstructure
Synchrotron radiation

ABSTRACT

Modification of the eutectic silicon in hypoeutectic Al–Si alloys causes a structural transformation of the silicon phase from a needle-like to a fine fibrous morphology and is carried out extensively in industry to improve mechanical properties. It has been documented that the fibrous silicon phase in chemically modified alloys is heavily twinned. It has been proposed that this increased density of twinning results from the adsorption of impurity-elements at the solid–liquid interface perpetuating further growth according to a twin plane re-entrant edge (TPRE) model. In this paper, we discuss this mechanism of eutectic modification in light of experimental data obtained by synchrotron radiation and predictions based on theoretical calculations. This research utilizes a μ-XRF (X-ray fluorescence) technique at the SPring-8 synchrotron radiation facility X-ray source and reveals that different elements which theoretically satisfy the geometric requirements of the impurity-induced TPRE model do not have the same effect on the growth of silicon during solidification. Europium for instance is distributed relatively homogeneously in the silicon phase while ytterbium was not found in the silicon phase at all. This has important implications for the fundamental mechanisms of eutectic modification in hypoeutectic aluminium–silicon alloys.

1. Introduction

The benefits of modification of the eutectic silicon phase in hypoeutectic Al–Si alloys are well known. The structural transformation of the silicon phase from a coarse plate- or flake-like structure to a fine fibrous structure improves the properties of cast components, in particular by increasing the tensile elongation. The fine fibrous eutectic modification of hypoeutectic Al–Si alloys that occurs when elements such as strontium and sodium are added has been explained based on observations of increased twinning. The increased density of twinning is believed to result from an impurity-induced twinning (IIT) mechanism which promotes further growth by encouraging the formation of a perpetuating twin plane re-entrant edge (TPRE)[1–4]. The high-density of twinning thereby imparts near isotropic growth to the silicon fibres which contrasts with the highly anisotropic growth typical of unmodified silicon flakes. The ideal size for an adsorbed atom to promote twinning was investigated by Lu and Hellawell [3] using a hard-sphere model for a twin event. Geometrically the ideal ratio of the atomic radii of the impurity-element compared to silicon (r_{ie}:r_{Si}) for an element to cause modification was calculated as 1.646 which falls reasonably close to the values of this ratio for known modifying elements (e.g. sodium, strontium, calcium and barium have rx (sub):rSi (sub) of 1.58, 1.84, 1.68 and 1.85, respectively). Fig. 1 and Table 1 show atomic radii for a range of elements and theoretically the best modification should occur by the addition of elements close to the proposed ratio (indicated by dashed line in Fig. 1). The microstructures of hypoeutectic Al–Si alloys containing Sr, Na, Ca, Ba and Eu have all been investigated by the authors and all contain silicon that is fibrous in morphology (1.65) [5–8]. Because the elements causing modification, including Na, Sr, Ba, Ca and Eu, all have an atomic radius ratio close to 1.65, the theory of IIT is generally well accepted.

In previous work the authors have investigated the micro-distribution of strontium, the most common modifying element, in the aluminium–silicon eutectic using μ-XRF and synchrotron radiation [9]. This technique was necessary as the low concentrations of strontium used for modification do not allow effective analysis using more conventional methods. Previous to this work the only successful study examining the interphase distribution of strontium was performed by selectively dissolving the aluminium and silicon eutectic phases and performing atomic absorption spectroscopy on the solutions [10]. The results of the μ-XRF analysis revealed strontium strongly segregates to the silicon phase and

* Corresponding author. Tel.: +61 7 3365 3919; fax: +61 7 3365 3888.
E-mail address: k.nogita@uq.edu.au (K. Nogita).

0925-8388/$ – see front matter © 2009 Elsevier B.V. All rights reserved.
doi:10.1016/j.jallcom.2009.09.138

Table 1
Physical and chemical properties of elements with potential eutectic modification.

Atomic number	Elements	Interatomic distance, r	r/r_{Si}	Meltng temperature (°C)	Boiling temperature (°C)	Enthalpy of fusion kj/mol	Enthalpy of atomization at 25°C kJ/mol	Ionic radius A	Oxidation states	Crystal Structure	Modification 0: needie 1 fibrous
11	Na	1.86	1 59	98	833	259	108.4	1020	1	bcc	1
20	Ca	197	1 68	839	1484	8 54	184.0	0 990	2	fcc	1
38	Sr	215	1.84	769	1384	9.16	163.2	1.120	2	fcc	1
39	Y	1.81	1.55	1526	3338	17.15	4180	0.900	3	hcp	0
51	Sb	1.45	1.24	631	1587	1987	263.6	0.760	3.5	Rhombohedral	1
56	Ba	218	1.86	729	1898	766	175.7	1.350	2	bcc	1
57	La	188	1.61	920	3457	620	4310	1061	3	hcp	0
58	Ce	1.83	1.56	798	3426	5.46	381.0	1.034	3.4	fcc	0
59	Pr	1.83	1.56	931	3512	6.89	368.0	1.013	3.4	hcp	0
60	Nd	1.79	1.56	1016	3068	7.14	322.0	0.995	3	hcp	0
61	Pm	180	1.54	931	3512	750	3100	0.979	3	hcp	0
62	Sm	1.79	1.53	1072	1791	862	209.0	0.964	3.2	Rhombohedral	0
63	Eu	1.99	1.70	822	1597	9.21	180.0	0.947	3.2	bcc	1
64	Gd	1.78	1.52	1312	3266	1005	352.0	0.938	3	hcp	0
65	Tb	1.76	1.50	1357	3023	1080	3140	0.923	3.4	hcp	0
66	Dy	1.75	1.50	1412	2562	1150	3010	0912	3	hcp	0
67	Ho	1.75	1.50	1470	2695	11.76	3010	0.901	3	hcp	0
68	Er	1.74	1.49	1522	2863	17.20	314.0	0.881	3	hcp	0
69	Tm	1.76	1.50	1545	1947	16.80	247.0	0.869	3.2	hcp	0
70	Yb	1.94	1.66	824	1194	7.66	180.0	0.858	3.2	fcc	0
71	Lu	173	1.48	1663	3395	18.70	398.0	0.848	3	hcp	0

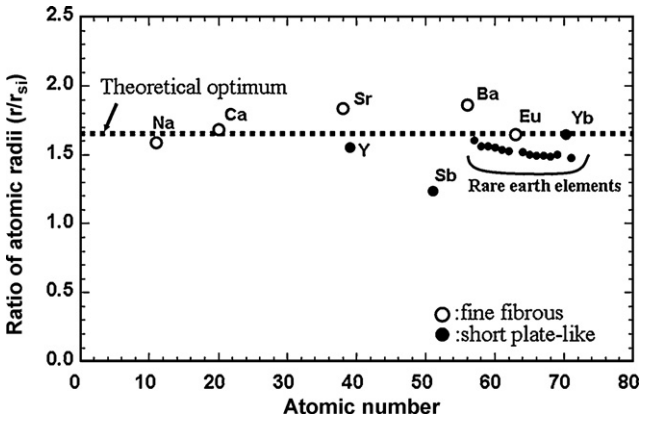

Fig. 1. Ratio of atomic radii vs. atomic number.

a small number of Sr-rich intermetallics and there was negligible concentration of strontium in the primary or eutectic aluminium phases. Importantly it was shown that Sr is distributed homogeneously in the eutectic silicon fibres. These observations support the impurity-induced twinning mechanism as a uniform distribution of the impurity-element would be expected throughout the silicon phase.

Among the rare earth elements, Eu and Yb have the most optimal ratios with r/r_{Si} of 1.70 and 1.66, respectively. The morphology of silicon in Yb modified samples has been variably reported as fibrous [3] or refined and needle-like [8]. Therefore, the IIT mechanism is somewhat controversial and there are published examples illustrating well-modified silicon fibres without a high-density of twins [11]. This paper investigates the trace Eu and Yb distributions in an Al—10 wt%Si by μ-XRF mapping in the SPring-8 synchrotron to further investigate the fundamental mechanisms of modification.

2. Experimental

The samples used in the experiments were Al—10 wt%Si alloys with 0–8,800 ppm and 0–13,900 ppm additions of Eu and Yb, respectively. The composition of the base alloy is given in Table 2. Eu and Yb were added as pure metals with 99.8% purity provided by Nippon Yttrium Co. Ltd. Japan. Castings were made in stainless steel cups shown in Fig. 2(a) with a thermocouple in the centre of the sample, 15 mm from the bottom, in order to monitor the temperature during solidification. A melt temperature of 720 °C was used throughout the study. The sample was placed in an insulating sleeve and allowed to cool, resulting in a cooling rate in the liquid at 610 °C, just prior to nucleation of the solid, of approximately 1 °C/s, and a total solidification time of approximately 300 s. Example of cooling curve is shown in Fig. 2(b). The castings were sectioned perpendicular to the axis of the cylinder, 15 mm from the bottom, and polished for metallographic and micro X-ray fluorescence microscope technique (μ-XRF) analysis.

The μ-XRF experiment was performed at an undulator beamline 47XU of SPring-8, Japan. Recently, a method for elemental mapping using a μ-XRF has been developed at the synchrotron radiation light source, SPring-8 Japan [9,12,13]. The spatial resolution is sub-100 nm, which is comparable to the current FE-SEM/EDX resolution. A schematic diagram of the experimental set-up is shown elsewhere [12,13]. The undulator radiation was monochromatized at 12 keV by passing through a liquid-nitrogen-cooled Si 1 1 1 double-crystal monochromator. A Fresnel zone plate was used as an X-ray focusing device to produce a fine probe. The FZP was fabricated by the electron-beam lithography technique at NTT Advanced Technology Co. Ltd. A zone structure with 1-μm-thick tantalum is deposited onto a 2-μm-thick SiC membrane. The diameter is 155 μm and the focal length at the X-ray energy of 12 keV is 150 mm. The outermost zone width is 100 nm. In this set-up, the beam size was 180 nm (vertical) × 150 nm (horizontal). The focused X-ray beam was used as the probe. The samples were mounted on a translation scanning stage with a motion accuracy of better than 10 nm. The XRF spectra were measured with a Si drift diode detector (Rontec Xflash D301).

First principles pseudopotential calculation of the energy penalty involved in substituting one M atom and a M–M pair for Al or Si has been carried out by the PAW method [14] with GGA functional parametrized by Perdew, Burke, and Ernzerhof [15,16] using VASP code [17,18]. This method only requires the atomic number and initial coordinates of atoms (no adjustable parameter). Energy is converged with respect to plane-wave cutoff, *k*-points, and FFT mesh, in which the error is much smaller than a few meV/atom and the energy difference calculated. Structure with or without substitution was fully optimized using a large supercell to minimize impurity–impurity interaction, and relaxation of structure around impurity atom is taken into account. From energy change of a supercell with substitution from that of reference state, the energy penalty to substitute one impurity atom for either Al or Si was calculated. This shows whether substitution is likely or unlikely, though these calculations did not taken into account any entropy contribution. Three impurity species, Sr, Er, and Yb, were surveyed for comparison with the experimentally determined μ (micro)-XRF distribution maps and Cu was investigated for reference purposes.

The energy penalty, ΔE, was calculated by

$$\Delta E = E^{\text{total}}_{\text{substitution}} - \left\{ E^{\text{total}}_{\text{reference}} - \mu_{\text{matrix}} + \mu_{\text{M}} \right\}$$

$E^{\text{total}}_{\text{reference}}$

$E^{\text{total}}_{\text{substitution}}$

where or is the total energy of the reference state or that of a state with substitution and μ_{matrix} or μ_{M} is the energy of an atom of matrix, either Al or Si, or energy of an impurity atom.

3. Results

Fig. 3 shows the eutectic growth temperatures taken from cooling curves obtained during the eutectic solidification of the unmodified (without Eu or Yb) and Eu and Yb containing samples. The reduction in eutectic growth temperature of more than 5 °C is typical of that which occurs with modification [4]. Fig. 4 shows optical micrographs of (a) unmodified, (b) 2400 ppm Eu and

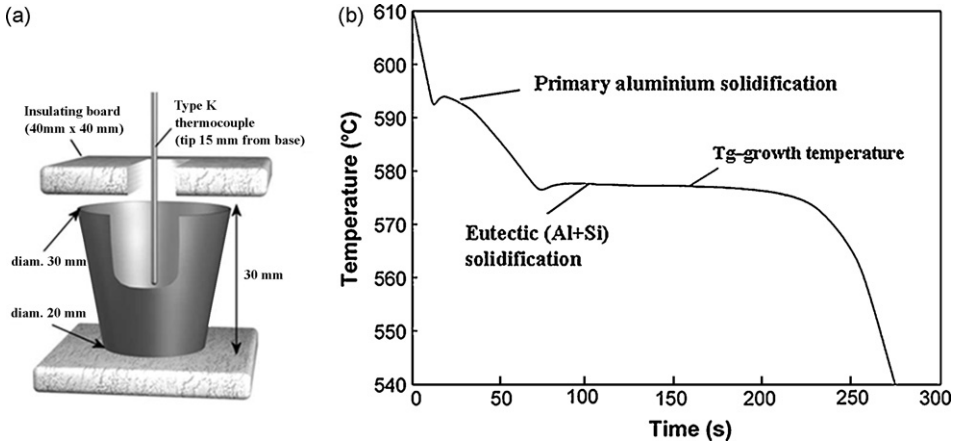

Fig. 2. (a) A schematic (cut-away and exploded for clarity) of the experimental set-up for thermal analysis. (b) The cooling curve showing the eutectic growth temperature for the sample.

Table 2
Average composition of the nominal Al—10 wt%Si alloy (wt%).

Al	Si	Cu	Fe	Mg	Zn	Cr	Ni	Mn	Ti	Sr	Zr	P
Balance	9.86	<0.01	<0.10	<0.01	<0.01	<0.005	<0.01	<0.01	<0.007	<0.001	<0.005	<0.002

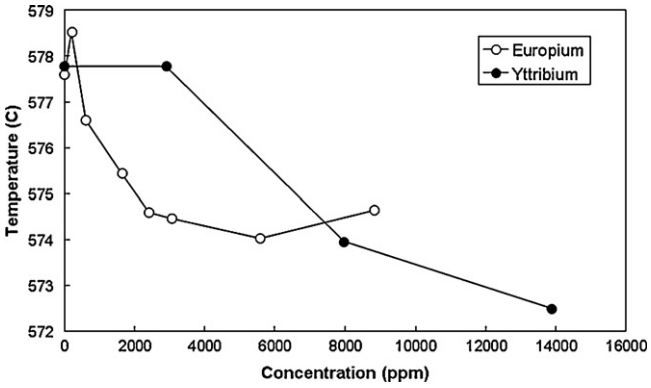

Fig. 3. Eutectic growth temperatures.

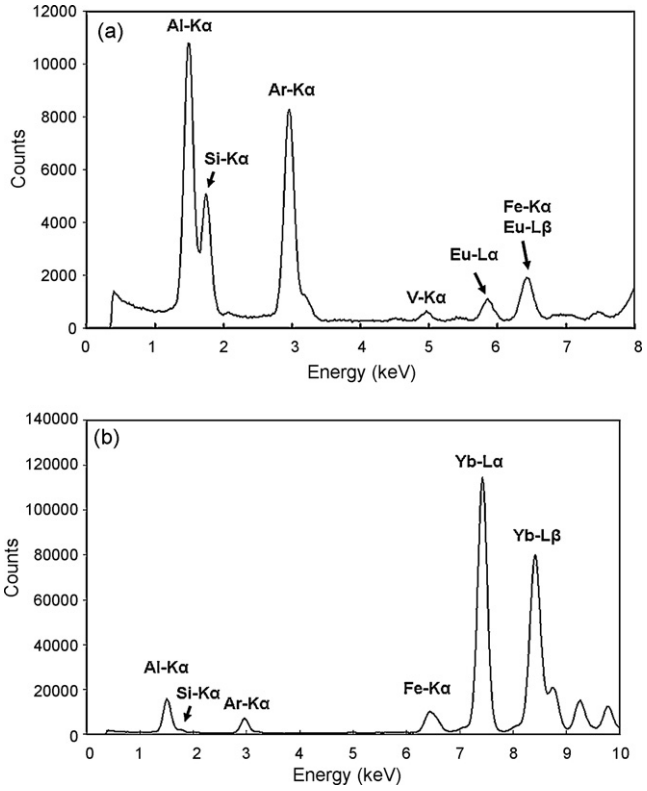

Fig. 5. a XRF spectra from Eu added sample. 5b XRF spectra of Yb precipitate from Yb added sample.

(c) 13,900 ppm Yb samples. As expected a coarse plate-like silicon morphology is observed in the unmodified sample as shown in Fig. 4(a), as is typical of aluminium–silicon alloys without any eutectic modification. The addition of 2400 ppm Eu resulted in a fully modified eutectic silicon phase with fibrous silicon morphology as shown in Fig. 4(b) with about a 4 °C relative drop in growth temperature. The structural transformation was limited to a refinement of the coarse plate-like silicon structure to a finer, but still plate-like morphology in the sample containing 13,900 ppm Yb as shown in Fig. 4(c).

The XRF spectra corresponding to the samples without and with Eu and Yb are shown in Fig. 5. The signal integration time for the acquisition of the XRF spectra was 200 s. Both spectra are taken from a region of approximately 50 μm × 50 μm incorporating aluminium dendrites, eutectic aluminium and eutectic silicon, and clearly indicate the presence of aluminium, silicon, and Eu or Yb. In the case of the 2400 ppm Eu sample, Eu $L_{\alpha 1}$ and $L_{\beta 1}$ (5.846 and 6.456 keV) are present. However, the energy of Eu $L_{\beta 1}$ is overlapping with Fe $K_{\alpha 1}$ (6.404 keV). Therefore, the elemental mapping of Eu for the analysis that follows has been taken from Eu $L_{\alpha 1}$. For the mapping of the 13,400 ppm Yb sample, Yb $L_{\alpha 1}$ (7.416 keV) has been used.

The μ-XRF elemental maps from the Eu sample of a eutectic region (containing eutectic aluminium and silicon) taken with a low magnification scan (scan pitch: 150 nm, signal integration time for each point: 1 s) are shown in Fig. 6(a–c), and a higher resolution map with fine-scan (scan pitch: 100 nm, integration time: 1 s) is shown in Fig. 7(a–c). It is clear from the mapping results that Eu is present in the eutectic silicon, and is of negligible concentration in the eutectic aluminium phase. This result is similar to previous results for Sr modification samples [9]. Figs. 8 and 9(a–c) show low magnification (Fig. 8, scan pitch: 1 μm, integration time:1.0 s) and high magnification (scan pitch: 200 nm, integration time:1.0 s) μ-XRF mapping of the Yb containing sample, respectively. In contrast to Eu, Yb is not present in silicon or aluminium but seems to have precipitated independently. The Yb in Fig. 9 is present just adjacent to the silicon phase.

Table 3 shows first-principal calculations of the differential of energy penalty to substitute one M atom, a M–M pair and a M-vacancy pair for the value of the difference between Al and Si ($\Delta\mu = \mu_{Al} - \mu_{Si}$). All the impurity atoms were more favourably dis-

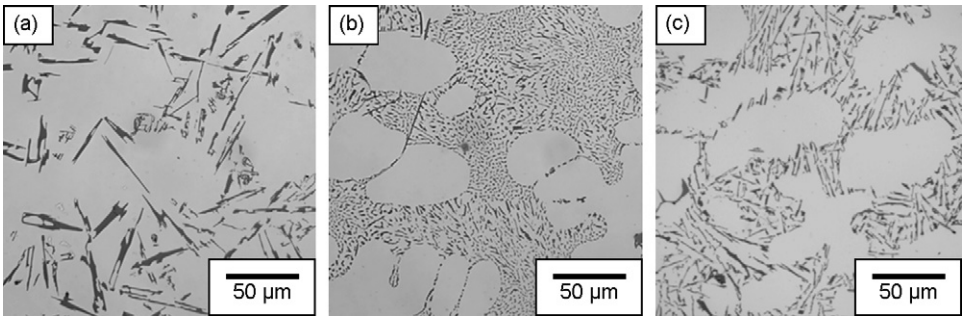

Fig. 4. Optical micrographs of fully solidified samples at the addition level corresponding to the maximum modification for the specified element; (a) unmodified, (b) 2400 ppm Eu and (c) 13,900 ppm Yb.

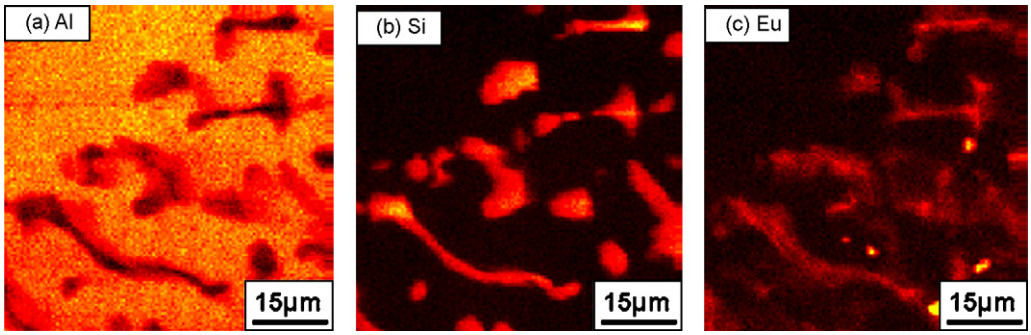

Fig. 6. μ-XRF mapping of Eu added sample taken by low magnification scan of (a) Al, (b) Si and (c) Eu (scan pitch: 150 nm, integration time:1.0 s).

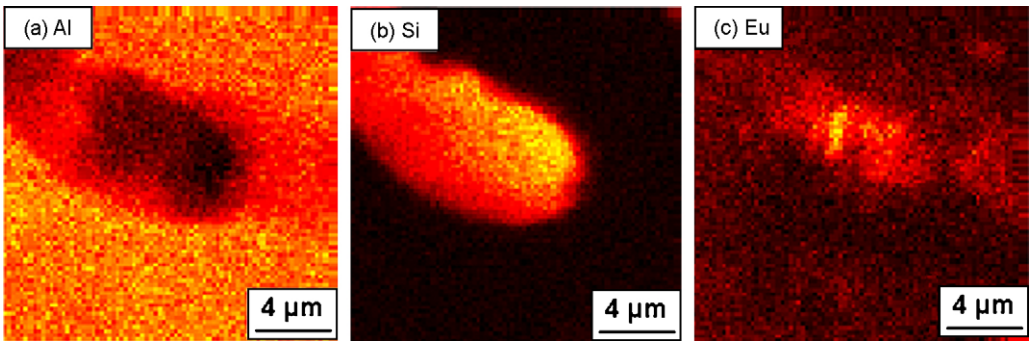

Fig. 7. μ-XRF mapping of Eu added sample taken by high magnification scan of (a) Al, (b) Si and (c) Eu (scan pitch: 100 nm, integration time:1.0 s).

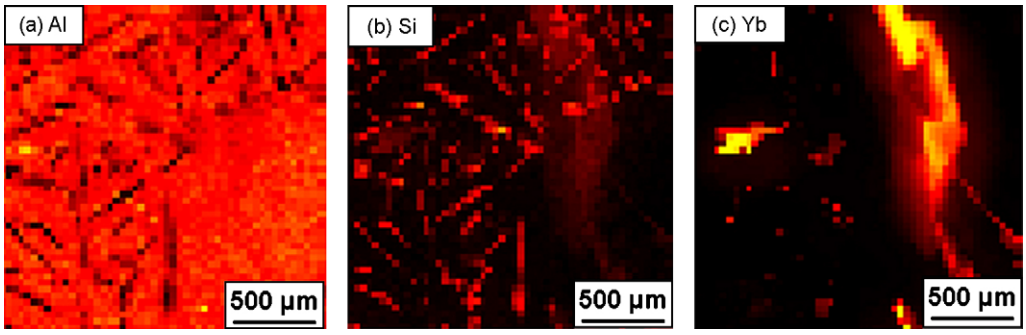

Fig. 8. μ-XRF mapping of Yb added sample taken by low magnification scan of (a) Al, (b) Si and (c) Yb (scan pitch: 1 μm, integration time:1.0 s).

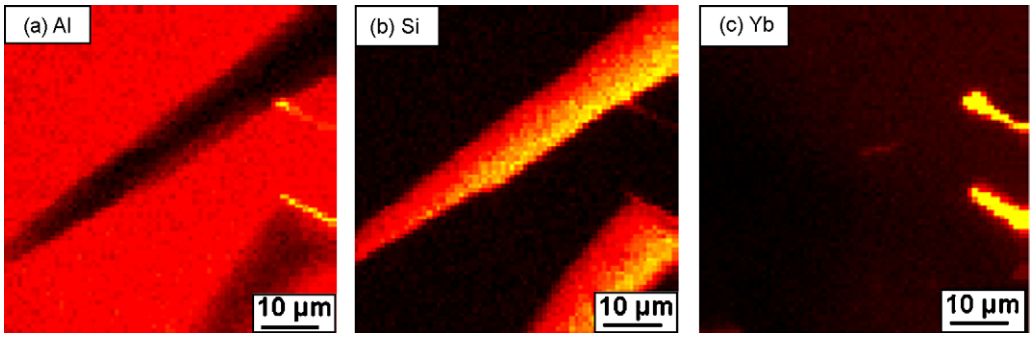

Fig. 9. μ-XRF mapping of Yb added sample taken by high magnification scan of (a) Al, (b) Si and (c) Yb (scan pitch: 200 nm, integration time:1.0 s).

Table 3
Differentials of energy penalty to substitute one M atom, a M–M pair and a vacancy-M pair for an Al or Si.

Element	Differencial of chemical potential of impurity atom doping, $\Delta\mu = \mu_{Al} - \mu_{Si}$(eV/atom)		
	Isolated atom	Atom-atom pair	Vacancy-atom pair
Sr	0.60	1.71	−0.93
Eu	2.90	1.51	−0.55
Yb	3.01	1.32	−0.51
Cn	2.28	1.02	0.21

solved into Al rather than Si when single or pair atoms without vacancies were considered. Dissolution of impurity atoms into Si as a dimer was energetically unfavourable for all kinds of impurity atom species studied. If a vacancy is introduced in Al and Si, however, the differential of energy penalty of all three elements was more favourable for Si. These results indicate that all three elements are less likely to dissolve in Si than Al but the tendency is reversed if vacancies are present in either phase. This implies that the presence of not only vacancies but also any kinds of lattice defects would reverse the tendency as well. It is noted that there is little difference in the predicted behaviours of Eu or Yb. The results for Cu show that this element is always found to have a preference for solid solution with Al in all scenarios investigated.

4. Discussions

The concept of the IIT mechanism, discussed briefly in the introduction, was developed to support TEM observations revealing high-density twinning within modified silicon fibres [2,19,20]. For the impurity strontium atoms to cause such a high-density of twinning would require them to be relatively uniformly distributed (at least finely dispersed on a sub-micron scale) throughout the silicon fibre as observed in the previous synchrotron μ-XRF mapping results. These results, therefore, lend support the operation of the IIT mechanism in modification of Al–Si alloys with Eu.

The fine fibrous eutectic structure that was obtained with Eu additions is typical of that obtained with conventional modifiers such as sodium and strontium [3]. As is commonly observed with Sr and Na, modification with Eu results in a significant depression of the eutectic nucleation and growth temperatures. Large additions of Yb, however, did not modify the eutectic silicon and only resulted in a small refinement of the plate-like morphology. Our previous works [6] showed 6400 ppm Yb resulted in a modified fine plate-like structure similar to the current Yb addition level of 13,900 ppm. Lu and Hellawell [3] reported significant eutectic modification with Yb, documenting results for an addition level of 5000 ppm. On the contrary, our results indicate that even at additions of 13,500 ppm Yb, fibrous modification does not occur and the silicon is still plate-like in spite of the prediction made by theoretical calculations mentioned above, although it is somewhat refined. We believed Yb modification results in a fine plate-like structure and that this structure is not the same as the fibrous modification seen with Sr or Na additions.

The behaviour of the majority of rare earth elements is, therefore, more similar to that of Sb than Sr or Na [5]. The refinement (as opposed to modification) of the plate-like silicon that occurs with Yb additions may be related to changes in the growth velocity that result from differences in the nucleation frequency of eutectic grains [21].

First-principal calculations indicate modifier elements are more likely to be present in the silicon phase only if there are vacancies present. This may relate to the existence of twin defects associate with modifier elements [1]. However, this does not explain why Yb was not detected in the Si phase as the analysis shows no difference between the behaviour of Eu or Yb.

Eu and Yb are within the atomic radii range predicted by previous models to be effective in producing growth twins on the silicon phase and are, therefore, predicted to result in modification. However, despite being of similar atomic diameter as Eu and having an atomic ratio of r/r_{si} close to the ideal ($r/r_{si} = 1.65$), Yb additions did not cause a flake-fibrous transition but only a refinement of the plate-like structure. This indicates that the ratio of atomic radii of a potential modifying element is not itself capable of predicting a fibrous transition in the eutectic silicon. It is likely that as suggested by Lu [3], properties such as the vapour pressure, tendency to form secondary compounds or oxides and phase equilibria with both the aluminium and silicon phases become important considerations. Based on synchrotron micro-XRF mapping results of modifier elements, we clarified Sr and Eu, which causes fine fibrous Si modification, are present within the eutectic Si, however, the atomic structures (single atom or cluster of modifier atoms or forming nano-domain intermetallics with Si) of modifier elements in Si are still unknown. We believe the chemical interaction between atomic scale defects in the eutectic silicon phase and modifier elements in combination with kinetic considerations may be the key for further understanding the mechanism of modification. Future research clarifying these structures may help elucidate the mechanisms of modification, and could be performed using synchrotron X-ray Absorption Fine Structure (XAFS) analysis.

5. Conclusions

Eu and Yb segregation in hypoeutectic Al–Si alloys has been investigated using μ-XRF in the SPring-8 synchrotron. The results show that Eu strongly segregates to the silicon phase and is of negligible concentration in the primary aluminium and eutectic aluminium phases. In addition, it has been shown that Eu is relatively homogeneously distributed in the eutectic silicon fibres. On the contrary, Yb precipitates and is not present at all in either Al or Si. These observations highlight the geometrically determined ratio of atomic diameter used to predict IIT behaviour is not sufficient when considered in isolation. It is also noted that, to-date, of the two studies that have been performed using μ-XRF show that all structures with fibrous modification have had the modifying element distributed homogeneously within the silicon phase.

Acknowledgments

The synchrotron radiation experiments were performed at SPring-8 with the approval of Japan Synchrotron Radiation Research Institute (JASRI) as Nanotechnology Support Project of the Ministry of Education, Culture, Sports, Science and Technology, Japan (Proposal No. 2008A1664/BL No. 47XU). Authors thank Mr. A. Nakamura, Osaka University for his SPring-8 synchrotron experiment support, and Mr. J. Read, The University of Queensland for his μ-XRF sample preparation. K. Nogita is funded by a Smart Futures Fellowship, Queensland Government, Australia.

References

[1] S.Z. Lu, A. Hellawell, J. Cryst. Growth 73 (1985) 316–328.
[2] L.M. Hogan, M. Shamsuzzoha, Mater. Forum 10 (1987) 270–277.
[3] S.Z. Lu, A. Hellawell, Metall. Trans. A 18A (1987) 1721–1733.
[4] J.E. Gruzleski, B.M. Glosset, The Treatment of Liquid Aluminum–Silicon Alloys, American Foundrymen's Society, Inc., Des Plaines, Illinois 60016-8399, U.S.A, 1990.
[5] K. Nogita, A.K. Dahle, Mater. Trans. 42 (2001) 393–396.
[6] K. Nogita, A. Knuutinen, S.D. McDonald, A.K. Dahle, J. Light Met. 1 (2001) 219–228.
[7] K. Nogita, S.D. McDonald, J.W. Zindel, A.K. Dahle, Mater. Trans. 42 (2001) 1981–1986.
[8] K. Nogita, S.D. McDonald, A.K. Dahle, Mater. Trans. 45 (2004) 323–326.
[9] K. Nogita, H. Yasuda, K. Yoshida, K. Uesugi, A. Takeuchi, Y. Suzuki, A.K. Dahle, Scripta Mater. 55 (2006) 787–790.
[10] L. Clapham, R.W. Smith, J. Cryst. Growth 92 (1988) 263–270.
[11] K. Nogita, J. Drennan, A.K. Dahle, Mater. Trans. 44 (2003) 625–628.
[12] A. Takeuchi, Y. Suzuki, H. Takano, J. Synchrotron Radiat. 9 (2002) 115–118.
[13] H. Takano, Y. Suzuki, A. Takeuchi, Jpn. J. Appl. Phys. 42 (2003) L132–L134.
[14] P.E. Blöchl, Phys. Rev. B 50 (1994) 17953–17979.
[15] J.P. Perdew, K. Burke, M. Ernzerhof, Phys. Rev. Lett. 77 (1996) 3865–3868.
[16] J.P. Perdew, K. Burke, M. Ernzerhof, Phys. Rev. Lett. 78 (1997) 1396–11396.
[17] G. Kresse, J. Hafner, Phys. Rev. B 49 (1994) 14251–14269.
[18] G. Kresse, J. Furthmüller, Phys. Rev. B 54 (1996) 11169–11186.
[19] L.M. Hogan, H. Song, Metall. Trans. A 18A (1987) 707–713.
[20] J.Y. Chang, H.S. Ko, J. Mater. Sci. Lett. 19 (2000) 197–199.
[21] S.D. McDonald, K. Nogita, A.K. Dahle, Acta Mater. 52 (2004) 4273–4280.